Nonequilibrium molecular dynamics simulations of transport and separation of gas mixtures in nanoporous materials

Lifang Xu, Muhammad Sahimi,* and Theodore T. Tsotsis
Department of Chemical Engineering, University of Southern California, Los Angeles, California 90089-1211
(Received 22 June 2000)

The nonequilibrium molecular dynamics simulations of transport and separation of a binary gas mixture through a porous membrane with interconnected pores of distributed sizes are reported. The membrane is modeled by a three-dimensional disordered *molecular* network of interconnected pores consisting of tens of thousands of atoms, based on a Voronoi tessellation of space. Results are presented for transport and adsorption of the gases, including the existence of an optimal pore structure for maximum separation of the gases.

PACS number(s): 47.55.Mh, 02.70.Ns, 05.60.Cd, 61.20.Ja

I. INTRODUCTION

Transport and separation of gaseous or liquid mixtures through technologically important porous materials, such as membranes, catalysts, and adsorbents, is a subject of great current interest [1,2]. These porous materials can, depending on their pore structure, contain a range of pore sizes, from nano- to meso- to micropores. However, the main resistance to the transport process is offered by interconnected nano- and mesopores. The small size of the pores also necessitates the use of molecular modeling. For example, since the average pore size of many membranes is typically of the order of a few angstroms, the traditional continuum approach [1] cannot be used for modeling such phenomena, and hence one must resort to molecular modeling. However, molecular simulation of transport and separation of a fluid mixture in a disordered pore space with interconnected pores is a formidable computational task. Because of this, and despite their technological importance, previous molecular studies of these phenomena have used only single pores, whereas the pore space morphology, i.e., the shape, size, and interconnectivity of the pores, as well as pore entrance effects and pore surface heterogeneity, all play important roles in determining the transport and separation properties of microporous materials.

In this paper we study, using molecular simulation, the transport and separation of gas mixtures in one class of nanoporous materials which are carbon based and have been gaining considerable attention. Carbon-based materials, such as carbon nanotubes, carbon nanoparticles, and carbon molecular-sieve membranes (CMSMs) have wide applications in many branches of science and technology. We focus here on CMSMs that are prepared by carbonization of polymeric precursors, and have been studied as a promising alternative to both inorganic (such as SiO_2 and metal) and polymeric membranes [3–6].

The molecular modeling methods are based on either equilibrium [7,8] or nonequilibrium molecular dynamics (NEMD) simulations. However, as is well-known, use of equilibrium MD (EMD) is not feasible for estimating the transport properties of mixtures in a system which, in a practical situation, is under the influence of an external potential (pressure, chemical potential, or concentration) gradient. NEMD techniques, such as the grand canonical molecular dynamics (GCMD) [9,10] and dual control volume GCMD (DCV-GCMD) [11–16], represent effective alternatives to EMD for such systems, and have been used for calculating the diffusivity of a single gas [11–14], as well as for mixtures of several gases [15,16], through a slit pore under the influence of an external potential gradient. Their extension to the technologically important phenomena of transport and separation of a fluid mixture through a real porous membrane, the pore space of which has a complex network of interconnected pores of various shapes and sizes, is nontrivial and, to our knowledge, has not been undertaken so far. This extension is, however, crucial to practical applications in which the affinities for adsorption of the various gases in a mixture greatly differ from each other, in which case their separation is not just by adsorption on the surface of the pores, but also by molecular sieving or due to the fact that some of the gases are transported across the membrane much faster than others, or a combination of all three mechanisms. While adsorption is mainly controlled by the porosity and surface area of the pore space, molecular sieving and transport of gases across the membrane are both controlled by the membrane's morphology, i.e., its pore size distribution and pore connectivity. Even when adsorption is the most important mechanism of separation, the pore space connectivity is still critical, because, while the pore space may have a large porosity, a large fraction of it can be isolated and inaccessible, in which case the way the pores are connected to each other is crucial. None of these effects can be accounted for by the single pore models.

The goal of this paper is to report the preliminary results of a molecular simulation of transport of gaseous mixtures in a nanoporous membrane in which the membrane is represented by a three-dimensional (3D) *molecular* pore network with interconnected pores. The pores have completely irregular shapes and sizes. We carry out EMD and NEMD simulation of transport and separation of a typical binary gas mixture—CO_2/CH_4—which is the focus of many studies, as it is encountered in many industrial and environmental problems, such as dealing with landfill gases.

*Author to whom correspondence should be addressed. Electronic address: moe@iran.usc.edu

The plan of this paper is as follows. In the next section we describe how the model of the pore space is generated. Section III contains a description of the NEMD simulation technique that we use in this paper. The results are presented and discussed in Sec. IV.

II. GENERATION OF THE MOLECULAR PORE NETWORK

To address the problem of representing the morphology of a nanoporous membrane by a realistic model, we have developed an algorithm for generating a molecular pore network. In our algorithm, we first create a 3D simulation box of carbon atoms with a structure corresponding to graphite. The reason for this is that, if the pyrolysis of the polymeric precursor is done at high enough temperatures, the resulting matrix of the pore space has a structure similar to that of graphite. We then tessellate the graphite box by inserting in it a given number of Poisson points each of which is the basis for a Voronoi polyhedron. Each polyhedron is that part of the box which is nearer to its Poisson point than to any other Poisson point. The pore space is created by fixing its desired porosity and then selecting a number of the polyhedra in such a way that their total volume fraction equals the fixed porosity. The polyhedra, so chosen, are then designated as the membrane pores by removing the carbon atoms inside them, as well as those that are connected to only one neighboring carbon atom (the dangling atoms), since it is impossible to actually have such atoms connected to the surface of the pores. The remaining carbon atoms constitute the membrane's solid matrix, while the pore space consists of interconnected pores of various shapes and sizes.

However, the pore space can be created by at least two different methods. If the pore polyhedra are selected at random, then, given that the size of the simulation box is large enough, their size distribution will always be Gaussian, regardless of the porosity of the pore space. This, however, is not very realistic from a practical viewpoint, because often the membranes that are used in practice do *not* possess a Gaussian pore size distribution (PSD) [6,16]. In the second method, one designates the pore polyhedra in such a way that the resulting PSD would mimic that of a real membrane, which is typically skewed [6,16]. To obtain such PSDs, we first sort and list the polyhedra in the box according to their sizes, from the smallest to the largest. The size of each polyhedron is taken to be its volume, or the radius of a sphere that has the same volume as the polyhedron. We then designate the polyhedra as the pores according to their sizes, starting from the smallest ones in the list. Figure 1 compares the PSDs of the pore networks generated by the two methods (more details about the simulations will be given shortly). The PSDs and their average pore sizes that are generated with the bias toward the smallest pores are of course dependent upon the porosity and resemble to some extent the experimental PSD [6,16]. Note that, unlike the traditional pore networks that are used in the simulation of flow and transport in porous media [1], the pore networks generated here are *molecular* networks in which the interactions of the gas molecules with *all* the atoms in the network are taken into account.

We must point out that in the type of molecular pore networks that are generated here, there is a difference between the ideal or total porosity, i.e., the total volume fraction of the pore polyhedra, and the *accessible* porosity, i.e., the volume fraction of the pores that not only can be reached by gas molecules from the membrane's surface, but can also accommodate the gas molecules, as some of the topologically accessible pore polyhedra may be too small to contain a gas molecule with a given finite size. In this sense, our definition of accessible pores is more restrictive than the one that is usually used in percolation theory [17,18]. In percolation theory, the mere connection of a pore to the outside surface of a membrane renders it accessible, whereas in the present problem the size of the transporting molecules is also important. Indeed, some of the pores may be accessible to one of the gases in a gaseous mixture, but too small to accommodate a much larger gas molecule in the same mixture, and in fact the molecular sieving property of a membrane is based and built upon this restricted accessibility.

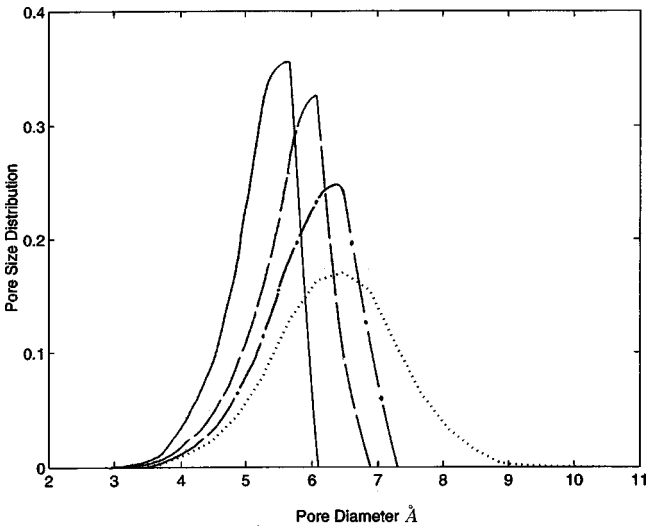

FIG. 1. Pore size distribution of the pore network for porosities 0.5 (solid curve), 0.6 (dashed), and 0.7 (dash-dotted). The dotted curve is the PSD when the pores are selected randomly.

Figure 2 presents the dependence of the accessible poros-

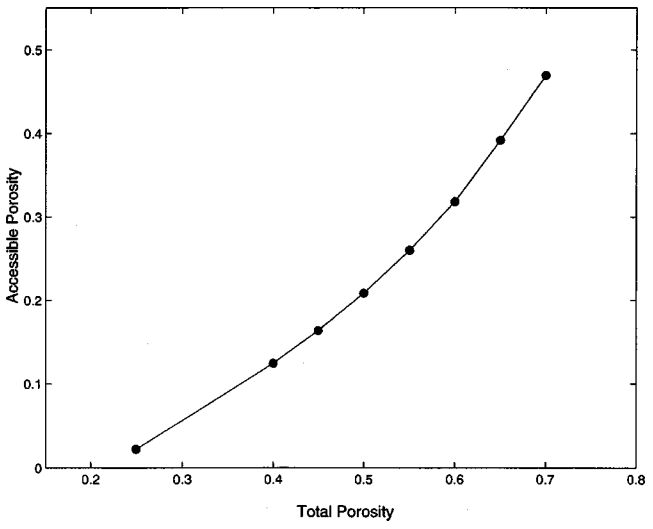

FIG. 2. Dependence of the accessible porosity on the total porosity.

TABLE I. Values of the LJ parameters used in the simulations.

Molecule	σ (Å)	ϵ/k (K)
CH_4	3.810	148.1
CO_2	3.794	225.0
C	3.4	28.00

ity on the total porosity. These results were obtained with the CH_4 molecules. However, since the kinetic diameters of CO_2 and CH_4 are close, the same results are essentially applicable to CO_2; the difference between the two cases is small. Note, for example, that for a total porosity of 0.5, the accessible porosity to CH_4 is about 0.22. If the size of all the pores is such that they can all accommodate the CH_4 molecules, then the percolation threshold of our molecular pore networks is the same as that of the traditional 3D Voronoi structure, which is about 0.16. However, if the PSD of the network is heavily biased toward the smallest pores, i.e., if a significant fraction of the pores are such that they cannot accommodate a gas molecule of a given size, then the percolation threshold of the network, *as far as transport of that gas is concerned*, is very different from that of traditional 3D Voronoi structures, and will in fact be *higher* than that of the Voronoi structure.

III. NONEQUILIBRIUM MOLECULAR DYNAMICS SIMULATIONS

As a typical and important binary gaseous mixture, we have studied transport, adsorption, and separation of CH_4 and CO_2 (components 1 and 2, respectively) and their binary mixtures. The two gases, as well as the carbon atoms, were assumed to be Lennard-Jones (LJ) hard spheres characterized by the LJ size and energy parameters σ and ϵ; the values we used are listed in Table I. For the cross-term LJ parameters the Lorentz-Berthelot mixing rule was used [7]:

$$\epsilon_{ij} = \sqrt{\epsilon_i \epsilon_j}, \tag{1}$$

$$\sigma_{ij} = (\sigma_i + \sigma_j)/2. \tag{2}$$

All the physical quantities were expressed in reduced units by using ϵ_{CH_4} and σ_{CH_4} as the basic units of energy and length. Table II lists the relation between the dimensional and dimensionless quantities. The carbon walls were assumed to be rigid and pairwise additivity was used describing the gas-gas and solid-gas interactions. The cut-and-shifted LJ 6-12 potential was used for describing the interactions between the gases, as well as between them and the carbon atoms,

$$U(r) = \begin{cases} U_{LJ}(r) - U_{LJ}(r_c) & \text{if } r \leq r_c \\ 0 & \text{if } r > r_c \end{cases} \tag{3}$$

where r_c is the truncation distance; we took $r_c = 5\sigma_{CH_4}$ for the LJ potentials, which proved to be very accurate. Here $U_{LJ}(r)$ is the usual LJ 6-12 potential:

$$U_{LJ}(r) = 4\epsilon\left[\left(\frac{\sigma}{r}\right)^{12} - \left(\frac{\sigma}{r}\right)^{6}\right]. \tag{4}$$

The interaction between the gas molecules and the *entire* carbon pore network was taken into account by calculating the sum of the LJ potentials between the gas molecules and each individual carbon atom in the network.

To impose a macroscopic potential gradient on the pore network in a given direction, we insert two control volumes (CVs), one each at the upstream and downstream positions of the network (in, say, the x direction). The two CVs are in equilibrium with two bulk phases that are kept at fixed upstream and downstream pressures or chemical potentials imposed on the network. The densities, or the corresponding chemical potentials in the CVs, were maintained constant by carrying out a sufficient number of grand canonical Monte Carlo (GCMC) insertions and deletions of the particles, with the probability p_i^+ of inserting a gas particle of type i being

$$p_i^+ = \min\{Z_i V_{ci} \exp[-(\Delta E/kT)/(N_i+1)], 1\}, \tag{5}$$

where $Z_i = \exp(\mu_i/kT)/\Lambda^3$ is the absolute activity at temperature T, Λ_i the de Broglie wave-length, μ_i the chemical potential of component i, ΔE the potential energy change resulting from creating or removing a particle, and V_{ci} and N_i the volume and number of atoms of component i in each CV, respectively. The probability p_i^- of deleting a particle is given by

$$p_i^- = \min\{N_i \exp[(-\Delta E/kT)/(Z_i V_{ci})], 1\}. \tag{6}$$

When a particle is inserted in a CV, it is assigned a thermal velocity selected from the Maxwell-Boltzmann distribution at the given T. An important parameter of the simulations is the ratio $\mathcal{R}$ of the number of GCMC insertions and deletions in each CV to the number of MD steps between successive GCMC steps. This ratio must be chosen appropriately in order to maintain the correct density and chemical potentials in the CVs, and also reasonable transport rates at the boundaries between the CVs and the pore space. In our simulations $\mathcal{R} = 50{:}1$ proved to be sufficient. Since the two CVs are well mixed and in equilibrium with the two bulk phases that are in direct contact with them, there should be no overall nonzero streaming velocity (ratio of the flux to the concentration of each gas component) in these regions. However, to reduce the numerical instability caused by the discontinuity of the streaming velocities at the boundaries between the CVs and the pore space, a small streaming velocity

TABLE II. The relation between the dimensional and dimensionless quantities (with an asterisk). k_B is the Boltzmann's constant.

Variable	Dimensionless form
Length L	$L^* = L/\sigma_{CH_4}$
Energy U	$U^* = U/\epsilon_{CH_4}$
Mass M	$M^* = m/M_{CH_4}$
Density ρ	$\rho^* = \rho\sigma_{CH_4}^3$
Temperature T	$T^* = k_B T/\epsilon_{CH_4}$
Pressure P	$P^* = P\sigma_{CH_4}^3/\epsilon_{CH_4}$
Time t	$t^* = t(\epsilon_{CH_4}/M_{CH_4}\sigma_{CH_4}^2)^{1/2}$
Flux J	$J^* = J\sigma_{CH_4}^3(M_{CH_4}/\epsilon_{CH_4})^{1/2}$
Permeability K	$K^* = K(M_{CH_4}\epsilon_{CH_4})^{1/2}/\sigma_{CH_4}$

was added to the thermal velocity of all the newly inserted molecules within each CV that were located within a distance $0.5\sigma_{CH_4}$ from the boundaries.

In the MD simulation of transport and separation of the gases in the pore network, the Verlet velocity algorithm [7] was used to solve the equations of motion. The time step Δt was adjusted according to the loading of the gas molecules and the average pore size, such that the standard deviations of the total energy relative to the mean was about 5×10^{-4} or less. A typical value of Δt selected in this way was 5×10^{-3} in reduced units, or 7.37×10^{-3} ps. To reduce the time for calculating the interaction between a gas molecule and all the carbon atoms, the simulation box was discretized into n^3 grid points with $n=111$, thus resulting in over 1 367 000 small subcells. We then used a 3D piecewise cubic Hermite interpolation [19] to compute the potential energy and forces for the gas particle at any position using the information at the n^3 grid points. Isokinetic conditions were maintained by rescaling the velocity independently in all three directions. During the MD calculations gas particles crossing the outer boundaries of the CVs were removed. In addition, we allowed for a nonzero streaming velocity (i.e., the ratio of the flux to the concentration of each gas component) in the entire pore space, consistent with the presence of bulk pressure/chemical potential gradients along the flow direction. The unrealistic assumption of a zero streaming velocity used in many of the single pore models leads to severely underestimated fluxes. The streaming velocity of each component in the pore space was obtained by linearly interpolating between its two values in the two CVs. Energy conservation in the system was monitored, and care was taken to ensure that the temperature of the system remained constant in order to eliminate any contribution of the temperature gradient to the transport. All the results reported here are for $T=25\,^{\circ}$C.

IV. RESULTS AND DISCUSSION

We first carried out some preliminary simulations using EMD in order to study the effect of the sample sizes. We investigated adsorption and self-diffusion of CH_4 in the pore space. Figure 3 shows the adsorption isotherms in terms of $\beta\mu_c$ versus loading (defined as the ratio of the total number of the gas molecules and the volume of the simulation box) for two different box sizes. Here $\beta=(k_BT)^{-1}$, where k_B is Boltzmann's constant, T is the temperature of the system, and μ_c is the chemical potential of CH_4 in the system. All the quantities shown in this and the following figures are dimensionless (see Table II for the relation between the dimensionless and dimensional quatities). The smaller box was $46.6\times39.6\times40.2\,\text{Å}^3$ in the x, y, and z directions, respectively (in the NEMD simulations, the external chemical potential or, equivalently, pressure gradient was applied in the x direction), while the size of the larger simulation box was $63.9\times63.95\times63.65\,\text{Å}^3$. For each sample size, the results for two different realizations are shown. The porosity in both cases was 0.5, and we used periodic boundary conditions in all three directions. As this figure indicates, up to a loading of about 0.3 there is very little difference between the two adsorption isotherms. While the difference between the two isotherms is larger at higher loadings, such high loadings are rarely encountered in practical situations. Moreover, the differences between the results for two different realizations with the same sample size are very small. Traditionally, the adsorption isotherms are represented as the loading versus the pressure in the system. Hence, Fig. 4 presents the adsorption isotherm, corresponding to Fig. 3, in this fashion. Since the atoms on molecules were assumed to be LJ hard spheres, the chemical potentials μ_c can be converted to the corresponding pressures using the equation of state for LJ fluids [20].

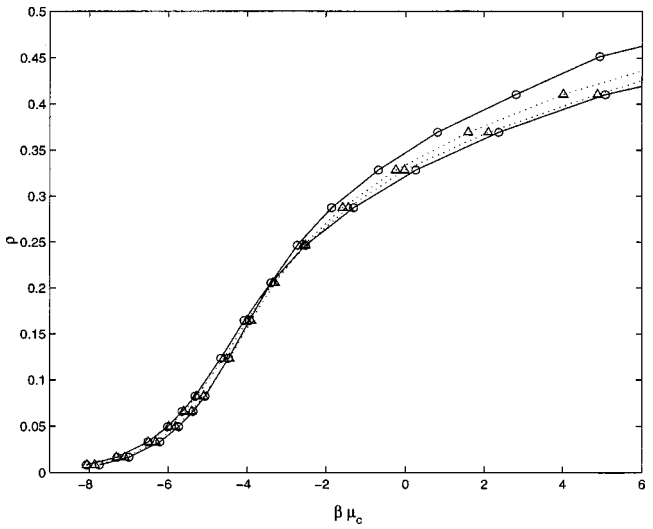

FIG. 3. Adsorption isotherms for CH_4. μ_c is the configurational chemical potential, while ρ is the loading. Circles and triangles show the results for the smaller and larger sample sizes, respectively (see the text for the sample sizes). The sample porosity is 0.5. All the properties are dimensionless (see Table I).

Figure 5 presents the self-diffusivity D of CH_4 versus loading at a porosity of 0.5 for the same two box sizes. For each size of sample we show the results for two different realizations of the pore space. Two important features are worth noting. One is that the self-diffusivity is much more affected by the sample size than is the adsorption isotherm. This is due to the fact that the pore space connectivity and PSD both strongly influence diffusion of a molecule in a

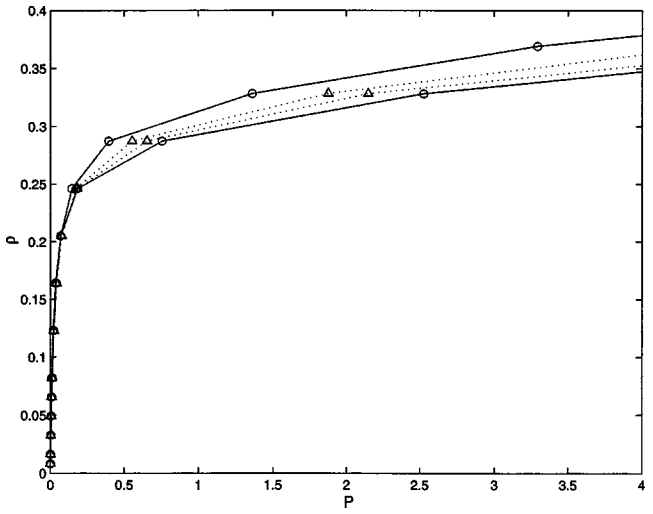

FIG. 4. Same as in Fig. 3, but versus the pressure P.

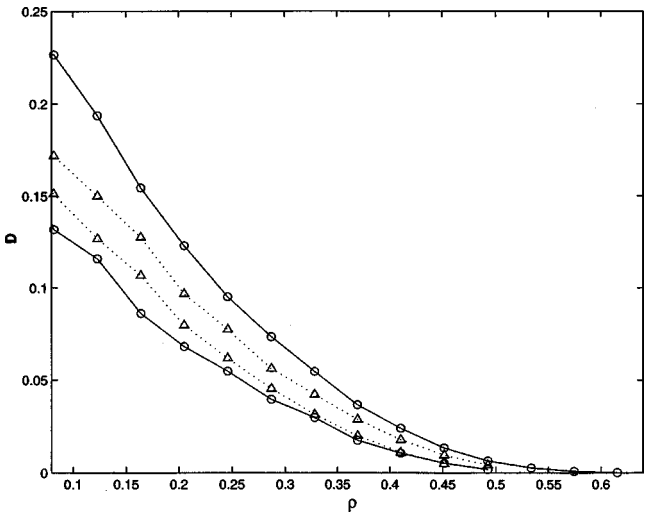

FIG. 5. Self-diffusivity D of CH_4 in the pore space (at a porosity of 0.5) versus loading. Symbols are the same as those in Fig. 3, and both D and ρ are dimensionless.

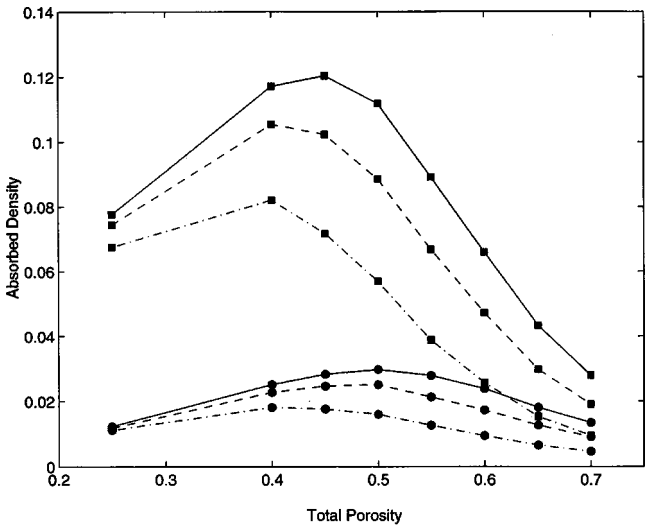

FIG. 6. Dimensionless adsorption isotherms for CO_2 (top three curves) and CH_4 (bottom three curves). The results are for the pressures 3 (solid), 2 (dashed), and 1 atm (dash-dotted).

pore space. The second noteworthy feature is that, while there are significant differences between the results obtained with the two different realizations of the pore space when the smaller sample is used, the difference decreases as the sample size increases. Moreover, we find that the lower the initial loading of the gas molecules, the more significant is the effect of their initial spatial distribution on the calculated properties.

Based on such EMD computations, we used the larger sample size in the rest of our studies. The results were also averaged over five realizations of the network and many initial distributions of the gas molecules in each realization. The number density of the carbon atoms was 114 nm^{-3} and the spacing between the adjacent graphite layers was 0.335 nm. The total number of initial carbon atoms in each realization was 29 640. The box was then tessellated into 1800 polyhedra. The average pore size for this pore network, the PSD of which is shown in Fig. 1, is about 6.4 Å, if the pore polyhedra are selected randomly. The average pore sizes when the pores are selected with the bias are 5.19, 5.63, and 5.92 Å for porosities of 0.5, 0.6, and 0.7, respectively. The mean pore size of typical CMSMs is about 3.5 Å [6]. A specific mean pore size is obtained by selecting an appropriate box size and then adjusting its number of Voronoi polyhedra. For example, with the same box size as the one we used in our simulation but with 11 600 polyhedra, the average pore size would be about 3.5 Å, if the pore polyhedra were selected randomly. This would require much more extensive computations, but also indicates the flexibility of our model.

Figure 6 presents the adsorption isotherms of CO_2 and CH_4, in an equimolar mixture, as functions of the pressure (in the pore space) and porosity. They indicate that the adsorbed amounts of the gases increase with increasing porosity, reaching a maximum at a porosity of about 0.45–0.5, beyond which they both decrease with increasing porosity. These results, to our knowledge, are completely novel. The maxima in the isotherms are due to two competing effects: A higher porosity provides more accessible pore surface area for adsorption, but at the same time decreases the interaction between the gas molecules and the pore surface, since a higher porosity also improves the interconnectivity of the pore space. The fact that CO_2 affinity for adsorption on a graphite surface is much larger than that of CH_4 has important implications. Since, relatively speaking, CO_2 is adsorbed on the pore surfaces in much larger amounts than is CH_4, its adsorption isotherm maxima are much more pronounced than those of CH_4. Thus, while the porosity has a strong effect on CO_2 adsorption, its effect on CH_4 is much weaker; the amount of adsorbed CH_4 varies only weakly as the pressure or porosity is varied. The important implication of the maxima in the adsorption isotherms is that there is an optimal pore space morphology (the distribution of the porosity and pore connectivity) for separation of gases in the membrane (see also below). These effects, which are absent in the single pore models, point to the significance of the pore space morphology in gas separation.

To study the separation properties of the membrane we calculate, after the system has reached steady state, the permeability K_i of gas i defined as

$$K_i = \frac{J_i}{\Delta P_i / L} = \frac{L J_i}{\Delta P_i}, \tag{7}$$

where $\Delta P_i / L$ is the partial pressure gradient for gas i along the membrane. The most interesting property is the dynamic separation factor,

$$S_{21} = \frac{K_2}{K_1}, \tag{8}$$

and its dependence on the membrane's pore space morphology. We utilized total pressures of 3 and 1 atm in the upstream and downstream bulk phase regions, respectively, the same as those used in our experiments with CMSMs using the same two gases [6,16]. Figure 7 shows the porosity dependence of S_{21} and the fluxes for an equimolar mixture of CO_2 and CH_4, indicating that they are both small at low porosities, which is due to two important factors: (1) small pore surface area for CO_2 adsorption, and (2) tortuous trans-

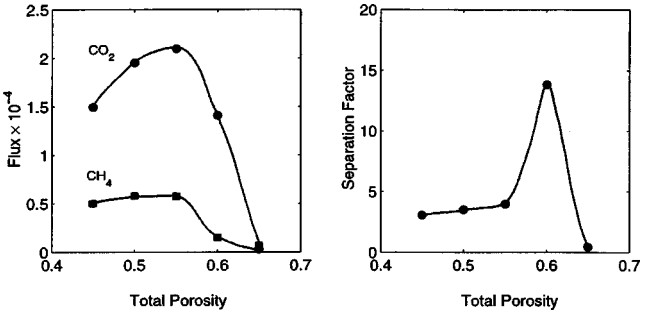

FIG. 7. Porosity dependence of the component (dimensionless) flux (left) and the separation factor (right).

port paths for CH_4, which is adsorbed much less than CO_2. However, as the porosity increases, the CO_2 flux also rises sharply, while the CH_4 flux remains essentially constant. Therefore, S_{21} also increases rapidly, reaching a maximum of about 14 at a porosity of about 0.6, which is consistent with the experimental data [6], after which it decreases almost as sharply as the porosity increases further. That membrane separation of the gases at high porosities is not effective is due to the presence of very large pores, which can no longer separate the two gases by molecular sieving.

It is instructive to compare these results with those obtained with the same gases in the single pore model [15,16]. The separation factors that are obtained with the single pore model are two orders of magnitude smaller than those of the experimental data [6], even when the pore size is the same as the average pore size of the membrane, whereas the results presented here are much more closely consistent with the data. Moreover, the separation factors depend on the porosity of the membrane, a morphological property whose effect cannot be taken into account by the single pore model, but is easily accounted for by our model. Finally, for mixtures such as H_2-CH_4, in which both gases have very little affinity for adsorption on the surface of the pores, the single pore model completely breaks down [15,16], even in a qualitative sense, whereas our model would predict [21] separation factors that are at least in qualitative agreement with the data [6]. In a future paper [21] we will present the results of extensive EMD and NEMD simulations of binary and ternary gas mixtures in the molecular pore network model and compare the results with the experimental data, as well as investigating the effect of various factors that affect these phenomena, such as the temperature, the mixture composition, and the nature of the gases.

V. SUMMARY

We have developed a molecular pore network model for nanoporous materials based on Voronoi tessellation of the space. The model affords us the flexibility of generating pore size distributions for the membrane that resemble closely those of real membranes. In addition, the molecular pore network model points to the significance of the molecular size of the transporting gases in defining (and, by implication, measuring) the membrane's accessible porosity. We have carried out equilibrium as well as nonequilibrium molecular dynamics simulations of transport, adsorption, and separation of binary gas mixture in the model membrane, which indicate significant differences between our results and those obtained with single pore models.

ACKNOWLEDGMENTS

We are grateful to the National Science Foundation and the Department of Energy for partial support of this work.

[1] M. Sahimi, Rev. Mod. Phys. **65**, 1393 (1993); *Flow and Transport in Porous Media and Fractured Rock* (VCH, Weinheim, 1995).

[2] *Access in Nanoporous Materials*, edited by T. J. Pinnavaia and M. F. Thorpe (Plenum, New York, 1995).

[3] J. E. Koresh and A. Sofer, Sep. Sci. Technol. **18**, 723 (1983); C. Bourgerette, A. Oberlin, and M. Inagaki, J. Mater. Res. **7**, 1158 (1992).

[4] C. W. Jones and W. J. Koros, Ind. Eng. Chem. Res. **35**, 2999 (1996).

[5] M. B. Shiflett and H. C. Foley, Science **285**, 1902 (1999).

[6] M. G. Sedigh, W. J. Onstot, L. Xu, W. L. Peng, T. T. Tsotsis, and M. Sahimi, J. Phys. Chem. A **102**, 8580 (1998); M. G. Sedigh, L. Xu, T. T. Tsotsis, and M. Sahimi, Ind. Eng. Chem. Res. **38**, 3367 (1999); M. G. Sedigh, M. Jahangiri, P. K. T. Liu, M. Sahimi, and T. T. Tsotsis, AIChE J. (to be published).

[7] M. P. Allen and D. J. Tildesley, *Computer Simulation of Liquids* (Oxford University Press, Oxford, 1987).

[8] X. Yi, K. S. Shing, and M. Sahimi, AIChE J. **41**, 456 (1995); Chem. Eng. Sci. **51**, 3409 (1996); X. Yi, J. Ghassemzadeh, K. S. Shing, and M. Sahimi, J. Chem. Phys. **108**, 2178 (1998); J. Ghassemzadeh, L. Xu, T. T. Tsotsis, and M. Sahimi, J. Phys. Chem. B **104**, 3892 (2000).

[9] J. Ji, T. Caginn, and M. B. Pettit, J. Chem. Phys. **96**, 1333 (1992).

[10] A. Papadopoulou, E. D. Becker, M. Lupkowski, and F. van Swol, J. Chem. Phys. **98**, 4897 (1993); E. J. Maginn, A. T. Bell, and D. N. Theodorou, J. Phys. Chem. **97**, 4173 (1993); M. Lupkowski and F. van Swol, J. Chem. Phys. **95**, 1995 (1995).

[11] G. S. Heffelfinger and F. van Swol, J. Chem. Phys. **100**, 7548 (1994); A. P. Thompson, D. M. Ford, and G. S. Heffelfinger, *ibid.* **109**, 6406 (1998); Mol. Phys. **94**, 673 (1998).

[12] J. M. D. MacElroy, J. Chem. Phys. **101**, 5274 (1994); M. Sun and C. Ebner, Phys. Rev. A **46**, 4813 (1995).

[13] S. Furukawa, K. Hayashi, and T. Nitta, J. Chem. Eng. Jpn. **30**, 1107 (1997).

[14] R. F. Cracknell, D. Nicholson, and N. Quirke, Phys. Rev. Lett. **74**, 2463 (1995).

[15] L. Xu, M. G. Sedigh, M. Sahimi, and T. T. Tsotsis, Phys. Rev. Lett. **80**, 3511 (1998).

[16] L. Xu, T. T. Tsotsis, and M. Sahimi, J. Chem. Phys. **111**, 3252 (1999); L. Xu, M. G. Sedigh, T. T. Tsotsis, and M. Sahimi, *ibid.* **112**, 910 (2000).

[17] D. Stauffer and A. Aharony, *Introduction to Percolation Theory*, 2nd ed. (Taylor and Francis, London, 1992).

[18] M. Sahimi, *Applications of Percolation Theory* (Taylor and Francis, London, 1994).

[19] D. Kahaner, C. Moler, and S. Nash, *Numerical Methods and Software* (Prentice-Hall, Englewood Cliffs, NJ, 1989).

[20] J. K. Johnson, J. A. Zollweg, and K. E. Gubbins, Mol. Phys. **78**, 591 (1993).

[21] L. Xu, T. T. Tsotsis, and M. Sahimi (unpublished).